Available online at www.sciencedirect.com
ScienceDirect
Journal of Solid State Chemistry 180 (2007) 3172–3179
JOURNAL OF SOLID STATE CHEMISTRY
www.elsevier.com/locate/jssc

Condensed rare-earth metal-rich tellurides. Extension of layered Sc_6PdTe_2-type compounds to yttrium and lutetium analogues and to Y_7Te_2, the limiting binary member

Laura M. Castro-Castro, Ling Chen[1], John D. Corbett*

Department of Chemistry, Iowa State University, Ames, IA 50011, USA

Received 6 June 2007; received in revised form 13 August 2007; accepted 6 September 2007
Available online 19 September 2007

Abstract

Six isotypic R_6ZTe_2 phases have been synthesized in Ta at elevated temperatures and characterized by single crystal X-ray refinements for $R = Y$, $Z = Rh$, Pd, Ag, Y and for $R = Lu$, $Z = Cu$, Ag. All crystallize in the Sc_6PdTe_2-type structure, *Pnma*, $Z = 4$, $a \sim 21.5$ Å, $b \sim 4.1$ Å, $c \sim 11.4$ Å. The results can be viewed as the replacement of Te3 atoms in the parent isotypic Sc_2Te (or in the hypothetical Y_2Te or Lu_2Te analogues) by the above the Z, the Y example giving the new binary phase Y_7Te_2. The shorter (and stronger) metal-metal bonds concentrate in the region of metal (Z, Y) substitution, as revealed by larger integrated crystal orbital Hamilton population (ICOHP) values derived from linear muffin-tin-orbital (LMTO) calculations. Partial densities-of-states data for Y_7Te_2 reflect a similar behavior. Individual R–R bond distances are seen to deviate appreciably from the more fundamental overlap population measures for each.

Keywords: Crystal structure; Band calculations; Polar intermetallic salts; Isotypic R_6ZTe_2 phases; Substitution reactions in intermetallic phases; Binary Y_7Te_2 phase

1. Introduction

Examples of the solid-state chemistry of *binary* metal-rich cluster *halides* of, first, the group 4 elements, Zr especially, and then of the group 3 (rare-earth-metal, R) members have been very sparse. However, this chemistry of the early metals was greatly expanded in many unprecedented directions through the inclusion within the clusters of stoichiometric amounts of electron-richer interstitial atoms (Z) from among either the nonmetallic or metallic elements [1,2]. Surprisingly, transition metals afford some of the richest and most novel chemistry in this role. A comparable expansion of the chemistry of the binary metal-rich (and relatively electron-poor) rare-earth-metal *tellurides* was likewise accomplished when the later 3d, 4d, or 5d metals were included in the reactions. These again took up interstitial roles in the rare-earth-metal arrays, but these generally exist in very different structures from those of the halides [3]. An early and indirect forecast of these productive advances in the new chemistry of such mixed, metal-rich systems can be found in the exceptionally high stabilities among polar transition metal intermetallics first noted by Brewer and Wengert in the 1970s [4]; that is, in the unusually large enthalpy decreases associated with the formation of compounds between early and the late transition metals.

Appreciable divergences between the crystal chemistries of such group 3 vs. group 4 metal-rich compounds arise in part from the smaller number of metal-based electrons in the former, which diminishes the number of occupied bonding states and therewith both weakens the bonding and decreases the dimensionality of the metal–metal framework, for example, in Sc_8Te_3 [5,6] vs. Ti_8S_3 [7] and Ti_8Se_3 [8], and Sc_2Te [9] vs. Zr_2Te [10]. Incorporation of late transition metals in analogous ternary derivatives of

*Corresponding author. Fax: +1 515 294 6789.
E-mail address: jcorbett@iastate.edu (J.D. Corbett).
[1]Fujian Institute of Research on the Structure of Matter, Chinese Academy of Sciences, Fuzhou, Fujian 350002, PR China.

0022-4596/$ - see front matter © 2007 Elsevier Inc. All rights reserved.
doi:10.1016/j.jssc.2007.09.012

group 3 metals stabilizes and diversifies these systems considerably. Many of the recently reported transition-metal-rich tellurides have common structural motifs, tricapped trigonal prisms (TCTP) of the early cluster metal (R) that are centered by a late transition metal Z (TCTP-Z). Diverse structure types among the tellurides are constructed from such fundamental building blocks via different condensation schemes. Three examples are the hexagonal series R_6ZTe_2 (R = Sc [11,12], Dy [13]; Z = Mn, Fe, Co, Ni, Ru, Rh, Os, or Ir), which are all ordered ternary variants of the very diverse Fe_2P-type family, and the orthorhombic $R_7Ni_2Te_2$ types, R = Er [14], Lu [15]; Z = Ni, Ru, or Pd. The former group includes the remarkable and so far unique Lu_8Te [16] in this structure type that is achieved on further substitution of Lu on Te sites.

In contrast, only a few analogues of the polytypic orthorhombic series Sc_6ZTe_2 (Z = Pd [17], Cu, Ag, Cd [18]) (*Pnma*) have been reported. Here, the formation of novel rumpled polycationic sheets (separated by Te anions) can be imagined to result from the insertion of, originally, Pd into a former Te site between the two types of metal columns in Sc_2Te [7]. At present the few Z atoms known to stabilize this R_6ZTe_2 polytype are among the electron-richer possibilities compared with those in the hexagonal series above. In addition, discovery of additional examples of the Sc_2Te parent structure has been sporadic and is presently limited to Gd_2Te and Dy_2Te [19].

In a wider view, the formation of hexagonal (Fe_2P derivative) members vs. the latter orthorhombic Sc_6ZTe_2 polytypes evidently cannot be readily extrapolated to other R and Z because the relative stabilities of competitive equilibrium R–Z phases that may naturally limit what R_6ZTe_2 can be obtained change with both R and Z. This particular problem arises in these systems because variations among diverse R_mZ_n alternatives depend on both R and Z, in contrast to R_vTe_w options that seem fairly monolithic. The former are known to be particularly dependent on Z, even for neighbors in the same period, presumably because of their changing electronic configurations. In fact, the stability or bonding variations within a given R_6ZTe_2 structural series, neglecting the alternatives, may depend on R and Z electronic configurations to a lesser degree, in part because all of these phases are metallic (have open bands), but much evidence for this beyond Sc examples has been lacking.

Here we report six new orthorhombic R_6ZTe_2 examples discovered on extension of our explorations to Y and Lu. (Of course, there were other R–Z combinations that were not productive, and these will not be detailed.) Yttrium has hitherto been an uncommon participant in the cluster telluride chemistry relative to Sc, either as binary tellurides or ternary phases with transition metals [5,20]. The sole published example of a yttrium ternary of this type is the unusual alternate, orthorhombic Y_5NiTe_2 [17,21] (*Cmcm*) which contains sheets of Ni-centered columns of Y that have been condensed side-by-side, a distinctly different motif from the isolated columns of Sc found in the Sc_5NiTe_2 polytype (*Pnma*) [22]. (This structural contrast may be rationalized in terms of R–R vs. R–Z bond energy differences [17]). Moreover, the discovery of the new isopointal Y_7Te_2 phase in this exploration is surely unifying. This structure can be derived by the equivalent of the oxidative insertion of Pd into the known Sc_2Te that originally yielded Sc_6PdTe_2 (above). Here, formal replacement of that Pd in the new Y_6PdTe_2 (or with other Z in five other examples) by a Y atom yields $Y_6(Y)Te_2$, although in this case the equivalent Y_2Te precursor has not been achieved and is evidently thermodynamically unstable.

2. Experimental section

2.1. Syntheses

All materials were handled in He- or N_2-filled gloveboxes. All syntheses started with the elements Y, Lu, (99.95% total, Ames Laboratory.), Cu, Ag (99.7% Fisher) or Ru, Rh, Pd powders (Alfa, >99.5% metals basis), and Te powder (99.99% Alfa-AESAR). In order to lower the activity of Te in the reactants, and its reaction with the Ta container during subsequent high temperature reactions, syntheses generally began with the preparation of the corresponding R_2Te_3 (disordered NaCl-type) or RTe from the weighed elements sealed in evacuated silica tubing. As before [11–14], these plus appropriate amounts of R and Z on a ~400 mg scale to give R:Z:Te = 6:1:2 stoichiometries were pressed into 1/4-in diameter pellets within a glovebox with the aid of a hydraulic press (Specac). The pellets were then arc-melted within the same box for 20 s per side at a current of 40 amp, turned over, and re-melted to improve homogeneity. Weight losses during arc-melting were <10%. Guinier patterns (below) from stoichiometric reactions in Ta at this point often revealed ~80% or better yields of orthorhombic R_6ZTe_2, with RTe as common minor impurity. In order to grow better single crystals and to obtain products that were at equilibrium at lower temperatures, the arc-melted buttons (wrapped with an intermediate Mo foil in order to lessen loss of Z, especially into the container) were resealed into Ta and then into evacuated fused silica jackets. These were subsequently annealed at 950–1050 °C for about 2 weeks, where after they were cooled, slowly to 800 °C and then radiatively to room temperature. Of course, reactions that omitted the arc-melting step required very significantly longer annealing periods to achieve the same results. Some loss of Z occurred in reactions run at 1300 °C. Most R_6ZTe_2 phases were so obtained in high yields, with small amounts of RTe (NaCl-type) often also being present (5–10%), probably because of the loss of Z. The high yields offer strong support for the assigned fixed stoichiometries. The compound Y_6PdTe_2 appeared to be stable in air at room temperature for weeks.

Single crystal refinements are presented and discussed below for (a) Y_6ZTe_2, Z = Rh, Pd, Ag, Y and (b) Lu_6ZTe_2,

Z = Cu, Ag. The initial discernment of Y_7Te_2 instead of certain targeted Y_6ZTe_2 phases by means of X-ray powder pattern data alone required some care. Other isostructural phases that have been synthesized and identified semi-quantitatively from powder patterns of mixtures but not structurally quantified are Y_6ZTe_2, Z = Ru, Os, Ir, Pd, Pt, Cu and also Sc_6PtTe_2. There is, however, some possibility that the usually smaller Y_7Te_2 might have been initially mistaken for the ternary target with the smaller Cu interstitial.

2.2. Powder X-ray diffraction

Powder patterns were secured with the aid of a Huber 670 Guinier camera equipped with an image plate. The powdered samples were held between two Mylar films by means of a little petrolatum, and these were in turn held between the two Al rings of the sample holder. Data were collected over 15–60 min, depending on whether the needs were for identification or precision. The unit cell parameters listed in Table 1 were generally refined from Guinier data.

2.3. Single-crystal diffraction studies

Well-facetted crystals were selected under low magnification in a special glovebox and sealed within 0.3-mm i.d. thin-walled capillaries. Diffraction data were collected from these at room temperature with the aid of a Bruker APEX CCD-based X-ray diffractometer and Mo$K\alpha_1$ radiation. Some of the important crystal and data collection parameters obtained are listed in Table 1. The reflection intensities were integrated with the aid of the SAINT [23] subprogram, and absorption effects were corrected with the aid of SADABS [24]. Cell symmetries and systematic absences in the reflection data consistently indicated the orthorhombic space group *Pnma* (No. 62) expected for this structure type, and this was verified for all by their successful refinements. The structures were solved by direct methods and refined by full-matrix least squares on F^2 with the aid of SHELXTL-6.10 [25]. Low residual values and the small peaks in the final difference Fourier maps, Table 1, were all supportive of the common structure type originally defined for Sc_6PdTe_2 [17].

The atomic positional data and isotropic and anisotropic displacement values for the six structures are collected in Table 2. The atoms are numbered as in the original report with Pd, but the positional data sets have all been reduced to a common standard setting with TIDY [26], unlike in previous reports. A complete listing of nearest-neighbor distances is given in Table 3.

2.4. Theoretical calculations

The electronic band structure of Y_7Te_2 was calculated by TB-LMTO-ASA methods with the aid of the Stuttgart LMTO 47 [27] program. The radii of the Wigner–Seitz spheres were assigned automatically so that the overlapping potentials would be the best possible approximation to the full potential. No interstitial sphere was necessary within an 18% overlap restriction.

Table 1
Collection and refinement data for R_6ZTe_2 phases, *Pnma* (No. 62)[a]

Compound	Y_6RhTe_2	Y_6PdTe_2	Y_6AgTe_2	Y_7Te_2	Lu_6CuTe_2	Lu_6AgTe_2
Formula weight	891.05	895.06	896.50	877.57	912.38	956.67
Lattice parameters[b] a (Å)	21.643(3)	21.634(3)	21.865(3)	21.3282(5)	20.97(1)	21.147(7)
b (Å)	4.0890(6)	4.1065(6)	4.0733(6)	4.0562(9)	3.967(2)	4.002(1)
c (Å)	11.462(2)	11.486(2)	11.506(2)	11.401(2)	11.240(5)	11.275(4)
Volume (Å^3)	1014.3 (3)	1020.4(3)	1024.7(3)	986.31(4)	934.9(7)	954.1(6)
Z, density calc. (g cm^{-3})	4, 5.838	4, 5.826	4, 5.811	4, 5.910	4, 9.723	4, 9.836
Absorp. coeff. (Mo$K\alpha$) (mm^{-1})	41.055	40.957	40.939	46.403	70.979	69.375
F_{000}	1532	1536	1540	1508	2236	2308
Crystal size, mm.	0.06 × 0.04 × 0.02	0.13 × 006 × 0.02		*0.04 × 0.03 × 0.01*	0.045 × 0.037x.034	0.06 × 0.04 × 0.02
Theta range for data, deg.	1.88–23.25	1.88 to 28.27	1.86–28.20	1.91–23.58	1.94–28.05	1.93–28.27
Index range	$-21 \leqslant h \leqslant 24$	$-19 \leqslant h \leqslant 28$	$-28 \leqslant h \leqslant 28$	$-24 \leqslant h \leqslant 24$	$-27 \leqslant h \leqslant 27$	$-14 \leqslant h \leqslant 27$
	$-4 \leqslant k \leqslant 3$	$-5 \leqslant k \leqslant 5$	$-5 \leqslant k \leqslant 3$	$-4 \leqslant k \leqslant 4$	$-3 \leqslant k \leqslant 5$	$-4 \leqslant k \leqslant 5$
	$-11 \leqslant l \leqslant 12$	$-14 \leqslant l \leqslant 13$	$-13 \leqslant l \leqslant 14$	$-12 \leqslant l \leqslant 9$	$-14 \leqslant l \leqslant 13$	$-14 \leqslant l \leqslant 12$
Refl. collected, R_{ave}	4074, 0.0552	5336, 0.0543	6040, 0.229	4170, 0.160	5247, 0.0846	5651, 0.0858
Indep. obs. refl, ($I > 2\sigma$(I))	850	1345	1368	863	1235	1283
Completeness, %	99.3	92.6	94.7	99.8	95.3	94.8
Data/restraints/parameters	850/0/56	1345/0/56	1368/0/56	863/0/56	1235/0/56	1283/0/56
GOOF	0.969	1.128	0.915	0.998	1.077	1.069
$R1/wR2$ (obs.data)	0.0265, 0.0541	0.0376, 0.0825	0.0406, 0.0716	0.0462, 0.0960	0.0423, 0.0835	0.0417, 0.0856
$R1/wR2$ (all data)	0.0375, 0.0557	0.0470/0.0850	0.0624, 0.0859	0.0608, 0.0996	0.0663, 0.0892	0.0576, 0.0966
Extinct. coeff.	0.00045(6)	0.00030(9)	0.0026(2)	0.00031(8)	0.00015(4)	0.00044(5)
Max./min. in ΔF map (eB-/Å^3)	1.174, −0.935	1.717, −2.127	3.216, −3.389	2.106, −2.112	2.751. −3.009	4.903. −3.145

[a]Data collected at 295 K; SADABS absorption correction; full matrix refinement on F^2.
[b]Lattice constants refined from Guinier powder data.

Table 2
Positional and displacement ellipsoid ($Å^2 \times 10^3$) data for R_6ZTe_2 and Y_7Te_2 compounds[a]

Phase	*R*1	*R*2	*R*3	*R*4	*R*5	*R*6	*Z*[b]	Te1	Te2
Y_6RhTe_2									
x	0.1097(1)	0.1557(1)	0.2660(1)	0.4731(1)	0.3551(1)	0.0099(1)	0.4267(1)	0.2390(1)	0.1253(1)
Z	0.3270(1)	0.0367(1)	0.7524(1)	0.3812(1)	0.0735(1)	0.6140(1)	0.6428(1)	0.4579(1)	0.7762(1)
*U*iso	24(1)	23(1)	17(1)	27(1)	16(1)	24(1)	13(1)	15(1)	16(1)
*U*11	14(1)	21(1)	19(1)	33(1)	20(1)	20(1)	15(1)	16(1)	18(1)
*U*22	36(1)	34(1)	16(1)	26(1)	13(1)	28(1)	9(1)	13(1)	16(1)
*U*33	22(1)	13(1)	15(1)	24(1)	15(1)	24(1)	14(1)	15(1)	14(1)
*U*13	0(1)	−1(1)	−2(1)	13(1)	2(1)	−2(1)	3(1)	0(1)	−1(1)
Y_6PdTe_2									
x	0.1096(1)	0.1571(1)	0.2664(1)	0.4704(1)	0.3545(1)	0.0113(1)	0.4271(1)	0.2393(1)	0.1251(1)
Z	0.3332(1)	0.0363(1)	0.7557(1)	0.3809(1)	0.0759(1)	0.6123(1)	0.6445(1)	0.4702(1)	0.7781(1)
*U*iso	19(1)	14(1)	12(1)	16(1)	12(1)	18(1)	17(1)	10(1)	11(1)
*U*11	9(1)	11(1)	12(1)	18(1)	14(1)	15(1)	19(1)	11(1)	11(1)
*U*22	34(1)	25(1)	15(1)	20(1)	13(1) (1)	27(1)	17(1)	12(1)	14(1)
*U*33	13(1)	8(1)	8(1)	10(1)	9(1)	13(1)	14(1)	9(1)	7(1)
*U*13	0(1)	0(1)	1(1)	−5(1)	−2(1)	1(1)	−2(1)	0(1)	0(1)
Y_6AgTe_2									
x	0.1090(1)	0.1579(1)	0.2668(1)	0.4693(1)	0.3523(1)	0.0148(1)	0.4267(1)	0.2394(1)	0.1269(1)
Z	0.3363(1)	0.0389(1)	0.7576(1)	0.3805(1)	0.0783(1)	0.6125(1)	0.6466(1)	0.4715(1)	0.7795(1)
*U*iso	21(1)	16(1)	15(1)	17(1)	17(1)	23(1)	16(1)	15(1)	14(1)
*U*11	16(1)	16(1)	16(1)	19(1)	25(1)	23(1)	18(1)	18(1)	16(1)
*U*22	29(1)	19(1)	16(1)	16(1)	13(1)	29(1)	16(1)	12(1)	15(1)
*U*33	16(1)	12(1)	13(1)	16(1)	13(1)	18(1)	16(1)	15(1)	12(1)
*U*13	1(1)	−1(1)	0(1)	−3(1)	−5(1)	−1(1)	−2(1)	0(1)	0(1)
Y_7Te_2									
x	0.1097(1)	0.1564(1)	0.2659(1)	0.4719(1)	0.3553(1)	0.0098(1)	0.426(1)1	0.2391(1)	0.1249(1)
Z	0.3256(2)	0.0340(2)	0.7516(2)	0.3802(2)	0.0720(2)	0.6126(2)	0.6416(2)	0.4664(1)	0.7749(1)
*U*iso	26(1)	20(1)	17(1)	21(1)	17(1)	23(1)	14(1)	16(1)	16(1)
*U*11	11(1)	13(1)	14(1)	16(1)	17(1)	17(1)	10(1)	12(1)	12(1)
*U*22	41(2)	30(1)	19(1)	26(1)	16(1)	29(2)	14(1)	19(1)	16(1)
*U*33	27(1)	17(1)	19(1)	20(1)	18(1)	23(1)	16(1)	17(1)	19(1)
*U*13	0(1)	−1(1)	0(1)	4(1)	−2(1)	−2(1)	1(1)	−1(1)	0(1)
Lu_6CuTe_2									
x	0.1089(1)	0.1558(1)	0.2680(1)	0.4748(1)	0.3569(1)	0.0058(1)	0.4233(1)	0.2380(1)	0.1257(1)
Z	0.3116(1)	0.0279(1)	0.7370(1)	0.3793(1)	0.0595(1)	0.6126(1)	0.6363(3)	0.4548(2)	0.7665(2)
*U*iso	19(1)	12(1)	12(1)	15(1)	10(1)	19(1)	7(1)	10(1)	10(1)
*U*11	7(1)	9(1)	11(1)	12(1)	8(1)	12(1)	3(1)	7(1)	7(1)
*U*22	38(1)	19(1)	16(1)	20(1)	13(1)	25(1)	6(1)	14(1)	15(1)
*U*33	11(1)	8(1)	9(1)	14(1)	9(1)	20(1)	12(1)	9(1)	7(1)
*U*13	2(1)	−1(1)	−1(1)	5(1)	−1(1)	7(1)	4(1)	1(1)	1(1)
Lu_6AgTe_2									
x	0.1086(1)	0.1593(1)	0.2684(1)	0.4722(1)	0.3594(1)	0.0075(1)	0.4236(1)	0.2370(1)	0.1268(1)
Z	0.3183(1)	0.0288(1)	0.7396(1)	0.3779(1)	0.0621(1)	0.6113(1)	0.6362(3)	0.4571(2)	0.7677(2)
*U*iso	14(1)	10(1)	10(1)	16(1)	9(1)	16(1)	15(1)	9(1)	1 0(1)
*U*11	13(1)	14(1)	14(1)	20(1)	15(1)	15(1)	19(1)	11(1)	13(1)
*U*22	22(1)	12(1)	10(1)	14(1)	7(1)	18(1)	11(2)	7(1)	9(1)
*U*33	7(1)	4(1)	7(1)	15(1)	6(1)	16(1)	14(2)	8(1)	6(1)
*U*13	1(1)	0(1)	0(1)	−7(1)	0(1)	5(1)	5(1)	1(1)	1(1)

[a]Atom numbers defined as in Ref. [17].
[b]$Z = Y7$ in Y_7Te_2.

3. Results and discussion

3.1. Structural evolution

Fig. 1 contains equivalent [010] projections of the three isotypic *Pnma* structures so as to enable a better understanding of the results, namely, the formation of a series of Y_6ZTe_2 phases, their evolution with *Z*, and the relationships among the three isotypic examples that differ only through atom exchanges at one particular site. All views are projected down short *b*-axes of ~4 Å (the effective diameter of Te) along which all atoms lie on mirror planes

Table 3
Important distances (Å) in R_6ZTe_2 phases, *Pnma*[a]

	Y_6RhTe_2	Y_6PdTe_2	Y_6AgTe_2	Y_7Te_2	Lu_6CuTe_2	Lu_6AgTe_2
R1–R2	3.473(2)	3.548(2)	3.585(2)	3.471(8)	3.337(3)	3.4336(3)
R1–R3 ×2	3.486(2)	3.490(2)	3.514(2)	3.445(6)	3.362(3)	3.400(3)
R1–R5 ×2	3.570(2)	3.559(2)	3.552(2)	3.545(6)	3.495(4)	3.467(3)
R1–R6 ×2	3.366(2)	3.386(2)	3.438(2)	3.331(6)	3.232(4)	3.265(3)
R1–Z[a] ×2	3.042(2)	3.080(1)	3.086(1)	3.015(5)	2.876(3)	2.947(2)
R1–Te1	3.232(2)	3.224(2)	3.249(2)	3.194(6)	3.150(4)	3.134(3)
R2–R3 ×2	3.628(2)	3.648(2)	3.632(2)	3.607(5)	3.466(4)	3.463(2)
R2–Z[a] ×2	2.974(1)	3.013(1)	3.018(2)	2.952(7)	2.858(3)	2.923(3)
R2–Te1 ×2	3.161(1)	3.133(1)	3.128(2)	3.109(5)	3.096(3)	3.077(2)
R2–Te2	3.058(2)	3.045(2)	3.061(2)	3.029(7)	3.005(4)	3.023(3)
R3–Z[a]	(3.697)	(3.704)	(3.722)	(3.639)	(3.448)	(3.483)
R3–Te1 ×2	3.208(1)	3.209(1)	3.198(1)	3.181(5)	3.153(3)	3.167(2)
R3–Te1	3.313(2)	3.331(2)	3.345(2)	3.301(7)	3.234(3)	3.254(3)
R3–Te2	3.057(2)	3.068(2)	3.068(2)	3.026(7)	3.002(4)	3.011(3)
R4–R4 ×2	3.599(2)	3.653(2)	3.676(2)	3.607(6)	3.523(4)	3.601(3)
R4–Z[a] ×2	2.993(2)	3.036(2)	3.068(2)	2.985(5)	2.921(3)	2.981(3)
R4–Z[a]	3.162(2)	3.169(2)	3.200(2)	3.136(7)	3.084(3)	3.088(3)
R4–Te2 ×2	3.188(1)	3.143(1)	3.151(2)	3.106(4)	3.160(3)	3.151(2)
R5–R6 ×2	3.596(2)	3.580(2)	3.570(2)	3.551(6)	3.547(4)	3.498(3)
R5–Te1 ×2	3.130(1)	3.132(1)	3.112(2)	3.101(4)	3.046(3)	3.092(3)
R5–Te2 ×2	3.123(1)	3.132(1)	3.116(1)	3.106(5)	3.079(3)	3.076(2)
R6–R6 ×2	3.346(2)	3.333(2)	3.356(2)	3.300(6)	3.225(3)	3.225(2)
R6–Z[a]	3.317(2)	3.335(2)	3.375(2)	3.326(6)	3.310(3)	3.355(3)
R6–Te2	3.113(2)	3.113(2)	3.115(2)	3.073(6)	3.052(3)	3.078(3)

[a] $Z = Y7$ in Y_7Te_2.

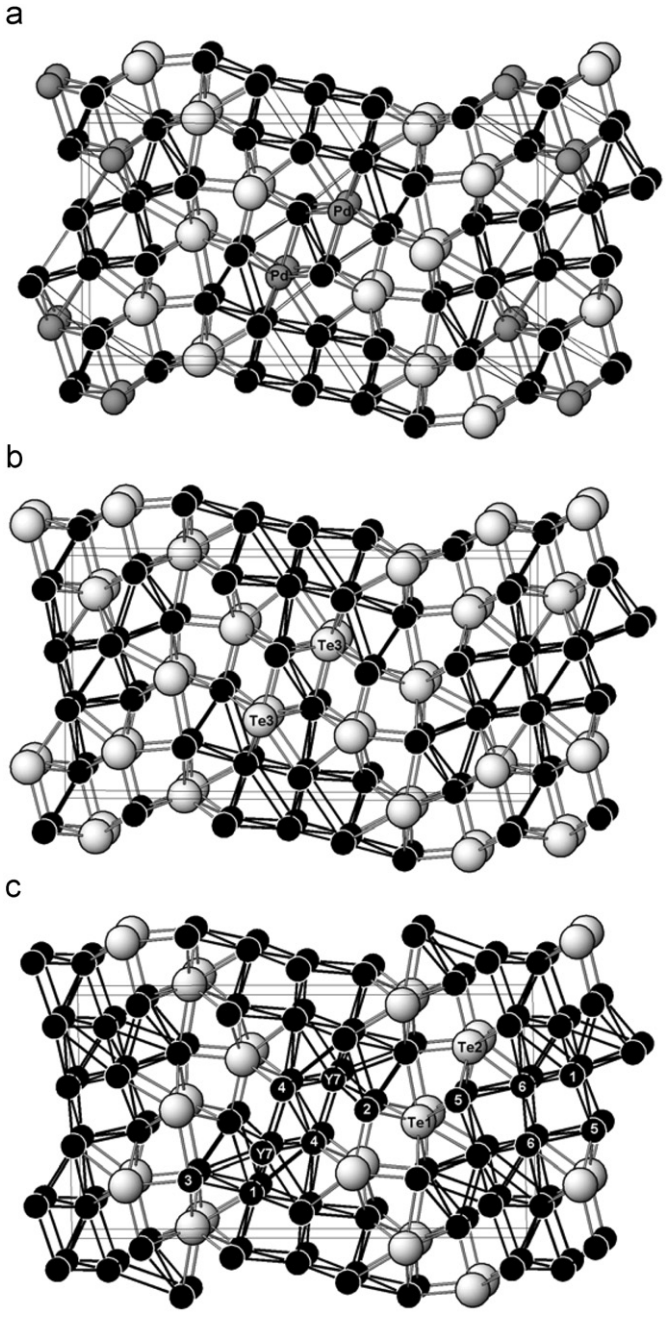

Fig. 1. ~[010] Views of the isotypic (a) Y_6PdTe_2, (b) hypothetical Y_2Te (after Dy_2Te), (c) Y_7Te_2, with Pd gray, Y black, Te white. The equivalent replaceable atoms are labeled Pd in (a), Te3 in (b), Y7 in (c). (The *a*-axis lies horizontal and to the right. An upper limit of 3.7 Å is used for bonds.).

at $y = 1/4$ or $3/4$. The Figure intercompares the structures of (a) Y_6PdTe_2, (c) Y_7Te_2 (Y_6YTe_2), and between these, (b) the hypothetical parent of both, "Y_2Te", isostructural with Sc_2Te as well as Dy_2Te and Gd_2Te. The differentiating atoms in the three known phases, with Pd, Te3, and Y7, respectively, are marked near the center of each drawing. The identities of all independent atoms are marked in the lowest Fig. (c); for further help, inversion centers lie on all cell edges, faces and at the origin and thence, at the centers of the Y4–Y4 and Y6–Y6 bonds.

The structures of all of three compounds, as typified by Y_6PdTe_2, Fig. 1a, contain as major building blocks comparable rectangular yttrium units first noted in Sc2Te [3,9] and seen here centered on all four edges of the *a–c* face of the cell. This geometry is more obvious after it is noted that neighboring Y atoms in these all alternate in projection by $b/2$. Thus the rectangular units can be derived from two semi-infinite columns of condensed Y octahedra defined by Y5,Y6 apexes and shared trans waist edges (Y1–Y6, lighter lines, Fig. 1a) that are further condensed via shared Y6–Y6 side edges. (See Fig. 1c for the atom numbers). [This rectangular column is further augmented by unusual trigonal prismatic Y2,Y3 units condensed onto Y1 at both ends to give aggregates that might be called "blades"]. The structure is completed by pairs of Z atoms (Pd, gray) that interconnect these blades and bracket the intervening Y4–Y4 zig–zag chains. The structure type is novel and interesting in part because the puckered Y metal sheets that result are separately fairly well by the large Te1 and Te2 atoms (anions), such that the closest Y–Y approach across the Te layers, d(Y3–Y5) ~3.90 Å, is notably larger than within the slabs, 3.4–3.6 Å. The former distance becomes even less meaningful with respect to bonding when it is noted that the d orbital energies of the outermost *R* atoms are raised and the *R–R* bonding (Mulliken overlap populations) between them therefore decreased according to the number of Te atoms that are bonded to each *R*. This is because *R*–Te covalency both lowers the energies of filled Te 5p orbitals and

"pushes up" the Y 4d valence orbitals on the neighboring outer atoms [5,11,17]. Further stages of Te replacement by *R* are known only for structures in which isolated Te atoms are bound within infinite 3D metal matrices, as in Lu_8Te, Lu_7Te and $Er_{17}Ru_6Te_3$ [28]. Beyond these lies a profusion of binary intermetallic *R*–*Z* phases.

The genesis of the ternary structure and the role of *Z* (Pd) is best seen by reference to the structure of the hypothetical "Y_2Te" in Fig. 1b, which is based on the real relationship between isotypic Sc_2Te and Sc_6ZTe_2 (*Z* = Pd, Pt, Ag, Cu, Cd). The Dy_2Te alone is dimensionally the better representation of Y_2Te as the single bond metallic radii differ by only 1% [29]. A point of particular note in the R_2Te structure type is the fairly isolated zig–zag chains of *R*4 (Y4). In this instance, their large number of Te neighbors and very low *R*4–*R*4 overlap populations [9,19] relative to the distances alone strongly suggest that the *R*4–*R*4 separation in the binary are determined more by their packing and bonding with tellurium than by significant electron densities in *R*4–*R*4 bonds. Notice also that each Y4 chain in b) is bridged to two adjoining Y "blades" by the Te3 atoms (renumbered here for consistency with R_6ZTe_2).

In accord with the known relationships with scandium [17], the oxidative displacement of those two Te3 atoms by Pd can be imagined to lead directly to the structure of Y_6PdTe_2 in a) via the conceptual process: $4Y_2Te + 2Pd \rightarrow Y_6PdTe_2 + 2YTe$. An appreciable reapportionment of distances and evidently of bonding is seen in the equivalent scandium structural pair at this stage in a general contraction around the inserted Pd; the Sc4–Sc4 distance decreases 0.10 Å and the formation of stronger Sc–Pd intermetal bonding seems evident. The latter bond types appear twice each to *R*4, *R*1 and *R*2, plus single Pd contacts with *R*4 and *R*6 that are (in comparison of the Sc and Y analogues, respectively) 0.10, 0.38 and 0.13, 0.30 Å longer and supposedly weaker (below). The *R*3–Pd distances are even greater, so that the Pd (vice Z, Te3) environment is better described as bicapped trigonal prismatic. (The *R* neighbors about Te1 and Te2 describe bi- and unicapped trigonal prisms, respectively, the major axis of the latter lying in the plane of the Figure.) The increases in *R*–Pd distances on transitioning from Sc to Y range from 0.17 to 0.27 Å, which compare reasonably well with a 0.18 Å difference in single bond radii [29]. (However, these bond standards may not be as useful in polyatomic systems with lower symmetry).

Comparisons among the distances in the variety of Y_6ZTe_2 examples, Table 3, as well as for those of the Sc and Lu analogues, give the general notion of a somewhat flexible *R*–*Z* network that accommodates size changes well. Lacking here is any sense of the larger picture, however; that is, what accounts for the lesser stability of unseen alternate products when a ternary does form with a particular *Z*, or what gives us any understanding of those binary (or higher) intermetallics that do form when R_6ZTe_2 products do not. Thus a simple reason is not clear as to why Sc_6ZTe_2 members do not form for *Z* to the left of Pd, Pt whereas Y_6ZTe_2 analogues do, other than "the stabilities of alternate phases".

There are difficulties as well in quantifying the bonding changes or differences among many examples, even by means of Table 3 and Fig. 1. We will later describe some calculational differences, but at this stage differences in Mulliken electronegativities give some indications of potential polarities and, presumably, bond strengths; namely, for Y, 3.19; Pd, Rh, Ag, 4.30 to 4.45; Te, 5.49 eV mol [30]. In addition, the introduction of d orbital bonding between *R* and the transition metal *Z* in place of covalent bonding with Te p orbitals alone evidently affords significant gains.

A remarkable and significant endpoint occurs with Y_7Te_2, Fig. 1c, a rare instance in which a binary phase is isotypic with the R_6ZTe_2 family for *Z* = Y. (Another could be taken to be Lu_8Te [16], which falls between the ternary hexagonal Fe_2P-type (literally Fe_6P_3) derivatives R_6ZTe_2 and h.c.p. Lu, in which the novel Lu_8Te has *Z* = Te in the 1*b* P site and Lu in the second 2*c* P (Te) site. Many other higher, ordered Fe_2P-type derivatives would also qualify.) In the limited range of available comparisons (Table 3), Y–Y bonds in Y_7Te_2 are persistently a little shorter than those in Y_6PdTe_2 except for *d*(Y7–Y6) which is substantially the same. (A marginally useful contrast in this case is that the Pd and Y single bond metallic radii differ by 0.33 Å [29]). At first thought, the stability of Y_7Te_2 might seem a little surprising without the avowed polar bond strength between the two 4d elements Y and Pd that were highlighted for Y_6PdTe_2, but d orbital bonding is retained, the orbital energy matching is better and, of course, *the competing phases are very different* without the presence of a late d element that could also form some *R*–*Z* product.

3.2. Bonding considerations

As noted before [9,22,31], interatomic distances in polar intermetallic "salts" such as these may in good part be determined as much by tight packing and atom sizes ("matrix effects") as by pair-wise "bonding" electron densities, as can be approximated by various means. We here extend earlier investigations of such matrix effects—that is, the contrasts if any between distances and relative measures of bonding in terms of overlap populations. In the present case, an ab initio DFT method, specifically a linear-muffin-tin-orbital (LMTO) means, allows better approximations of bond strengths via integrated crystal orbital hamilton population (−ICOHP) values [32]. (These in effect afford orbital energy corrections to the Mulliken overlap populations determined by extended Hückel methods [33].) The former reveal some significant contrasts in Y_7Te_2 and emphasize once again how inadequately distances alone reflect factors more closely related to bond strengths (bond populations).

First, Fig. 2a shows the LMTO results for Lu_7Te_2 as the total densities-of-states (DOS) and some partial

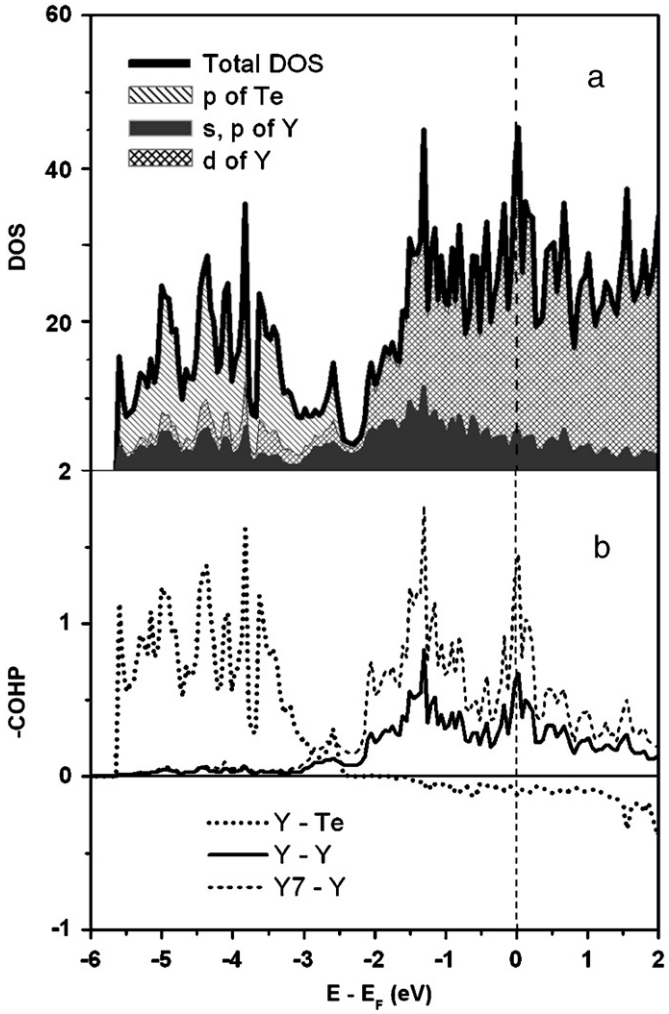

Fig. 2. (a): DOS and PDOS data for Y_7Te_2 from LMTO calculations (dashed line: E_F). The principal bonding contributions are Y 4d and Te 5p. (The PDOS are 'stacked' so the areas seen represent total relative contributions). (b) —COHP data per bond mol for Y–Te (dotted), all Y–Y (solid), and Y7–Y (dashed). The last two clearly reflect a greater-than-average population between Y7 and its neighbors.

contributions by various atomic orbitals (PDOS). (The a.o. contributions here are projected separately, without overlap.) The separation between Te 5p contributions below ~–2,5 eV and Y 4d above is clear but not unexpected. The Y s, p components are small but evident, whereas Te s contributions (not shown) are quite unimportant in this region. The—COHP data, Fig. 2b, also show the sizable differences as a function of energy between major Y–Te and Y–Y bonding. Particularly noteworthy with respect to the latter are the larger values per bond-mol for just Y7 to its Y neighbors (dashed line) vs. for all Y–(solid line). This more firmly supports inferences from distances that the Y–Y bonding is more concentrated in the neighborhood of Y7, which lacks any near Te neighbors as well.

Numerous contrasts between distances and their integrated—ICOHP values listed in Table 4 are evident. The three shortest bonds in Y_7Te_2, Y1–Y7, Y3–Y7 and Y4–Y7, have in parallel the largest –ICOHP values, although not

Table 4
Distance vs.—ICOHP data for Y_7Te_2

Bond	Distance (Å)	–ICOHP (eV mol)
Y1–Y2	3.47	0.622
Y1–Y3	3.44	0.522
Y1–Y4[a]	3.76	0.401
Y1–Y5	3.54	0.180
Y1–Y6	3.33	0.570
Y1–Y7	3.02	1.142
Y2–Y3	3.61	0.276
Y2–Y4[a]	3.83	0.115
Y2–Y7	2.95	0.918
Y3–Y5[a]	3.87	0.106
Y3–Y7	3.64	0.415
Y4–Y4	3.61	0.226
Y4–Y6[a]	3.68	0.242
Y4–Y7	2.98	1.239
Y5–Y6	3.55	0.075
Y6–Y6	3.23	0.276
Y6–Y7	3.33	0.771

[a]Longer distances not included in Table 3.

exactly in the same order. These are in the same locations as the three shortest Y–Pd distances in Y_6PdTe_2; yet they still mark the three largest distance contractions on going from Y_6PdTe_2 to Y_7Te_2 (Table 3), that is, around the site at which Te3 in "Y_2Te" has been replaced by Y7 with a gain in additional Y1–Y2 and Y1–Y4 interactions as well. (Heretofore, only overlap populations have been available for such comparisons with Sc_2Te and Dy_2Te.) The strong bonding effects (short distances) among *R*5, *R*6 and *R*1 that were especially evident in the condensed octahedral chains in Y_6PdTe_2 (as well as Sc_2Te and Dy_2Te [9,19]) have evidently shifted to the region around Y7.

These effects are further emphasized in Fig. 3 in a plot of separate Y–Y distances vs. their corresponding—ICOHP values in Y_7Te_2, those for (*R*–*R*) 6–6, 1–5, and 5–6 being the lowest in the 3.2 to 3.7 Å range and clearly below the mean curve. The lone low member among the highest—COHP values is for Y2–Y7, with the shortest separation in Y_7Te_2. These all fit fairly well with the evident source of the irregularity noted earlier, the effect of Te neighbors in diminishing *R*–*R* bonding capabilities by that particular *R*. The number of Y–Te distances below 3.15 Å are, for Y5, four Te; for Y2 and Y3, 3 each; Y4, two; Y1, Y6, one; Y7, no Te neighbors. This characteristic is qualitatively evident in Fig. 1c, Y2. Y3 and Y5 being more or less exterior atoms, somewhat isolated from the center of the Y–Y bonding. This source of reduced bonding seems clear for Y5 and reasonable for Y2–Y7, although that result still represents a good bond. As note earlier, distance changes on conversion between $Z = Pd$ and Y (Table 3) give the general impression that bonding around Y6 is in parallel reduced appreciably, and this is particularly evident theoretically for Y5–Y6 and Y6–Y6. Attribution of other differences to "matrix effects" is naturally vague and probably excessive, but the data again provide strong

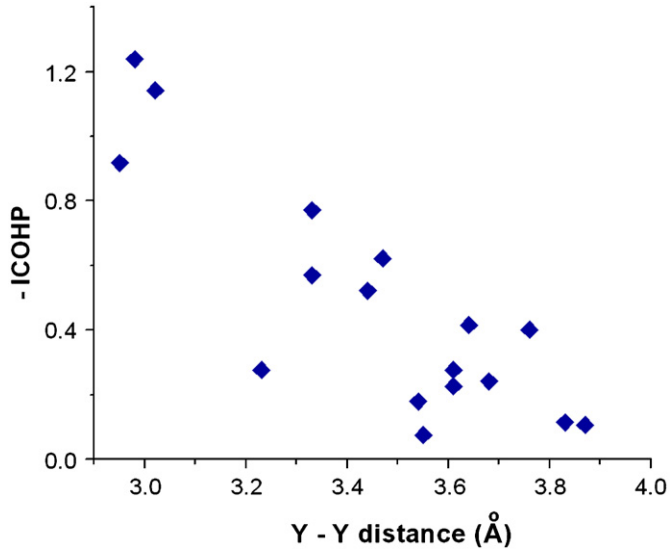

Fig. 3. –ICOHP data (eV/bond.mol) vs. distance (Å) for Y–Y contacts in Y_7Te_2 (Table 4).

indications that relative bond distances may not be good measures of something related to bond strengths, or at least overlap populations. The fact that *d*(Y6–Y6) doesnt increase even more really may be a very good example of a matrix effect, the atom "locked" into a 3D matrix.

Acknowledgments

We are indebted to Qisheng Lin for some of the graphics. This research was supported by the National Science Foundation, Division of Materials Research, under Grants DMR-0129785 and -0444657 and was performed in the facilities of the Ames Laboratory, US Department of Energy.

References

[1] A. Simon, Hj. Mattausch, G.J. Miller, W. Bauhofer, R.K. Kremer, in: K.A. Gschneidner, L. Eyring (Eds.), Handbook on the Physics and Chemistry of Rare Earths, vol. 15, Elsevier Science Publishers, Amsterdam, 1991, p. 191.
[2] J.D. Corbett, J. Alloys Compds. 418 (2006) 1.
[3] J.D. Corbett, in: G. Meyer, D. Naumann, L. Wesemann (Eds.), Inorganic Chemistry in Focus II, Vol. 2, Wiley-VCF, Weinheim, Germany, 2005 Chap. 8.
[4] L. Brewer, P.R. Wengert, Metall. Trans. 4 (1973) 83.
[5] P.A. Maggard, J.D. Corbett, Inorg. Chem. 37 (1998) 814.
[6] L. Chen, S.-Q. Xia, J.D. Corbett, Inorg. Chem. 44 (2005) 3057.
[7] J.P. Owens, H.F. Franzen, Acta Crystallogr. B 30 (1974) 427.
[8] T.E. Weirich, R. Pöttgen, A. Simon, Z. Kristallogr. 211 (1996) 629.
[9] P.A. Maggard, J.D. Corbett, Angew. Chem. Int. Ed. Engl. 36 (1997) 1974.
[10] G. Örlygsson, B. Harbrecht, Inorg. Chem. 38 (1999) 3377.
[11] P.A. Maggard, J.D. Corbett, Inorg. Chem. 39 (2000) 4143.
[12] L. Chen, J.D. Corbett, Inorg. Chem. 43 (2004) 436.
[13] N. Bestaoui, P.S. Herle, J.D. Corbett, J. Solid State Chem. 155 (2000) 9.
[14] M. Fanqin, T. Hughbanks, Inorg. Chem. 40 (2001) 2482.
[15] L. Chen, J.D. Corbett, Inorg. Chem. 43 (2004) 3371.
[16] L. Chen, J.D. Corbett, J. Am. Chem. Soc. 125 (2003) 7794.
[17] P.A. Maggard, J.D. Corbett, J. Am. Chem. Soc. 122 (2000) 10740.
[18] L. Chen, J.D. Corbett, Inorg. Chem. 41 (2002) 2146.
[19] P.S. Herle, J.D. Corbett, Inorg. Chem. 40 (2001) 1858.
[20] P.A. Maggard, Ph.D. Dissertation, Iowa State University, 2000.
[21] P.A. Maggard, J.D. Corbett, Inorg. Chem. 43 (2004) 2556.
[22] P.A. Maggard, J.D. Corbett, Inorg. Chem. 38 (1999) 1945.
[23] SAINT, Bruker AXS, Inc., Madison, WI, 2000.
[24] R.H. Blessing, Acta Crystallogr. A 51 (1995) 33.
[25] SHELXTL6.10, Bruker AXS, Inc., Madison, WI, 2000.
[26] L.M. Gelato, E.J. Parthé, J. Appl. Crystallogr. 20 (1987) 139.
[27] R. Tank, O. Jepsen, A. Burkhardt, O.K. Andersen, TB-LMTO-ASA program, Max-Plank-Institut für Festkörperforschung, Stuttgart, Germany, 1994.
[28] A. Mehta, J.D. Corbett, unpublished research, 2007.
[29] L. Pauling, Nature of the Chemical Bond, third ed, Cornell University Press, Ithaca, NY, 1960, p. 403.
[30] R.G. Pearson, Inorg. Chem. 27 (1988) 735.
[31] P.A. Maggard, J.D. Corbett, J. Am. Chem. Soc. 122 (2000) 838.
[32] R. Dronskowski, P. Blochl, J. Phys. Chem. 97 (1993) 8617.
[33] W. Glassey, R. Hoffmann, J. Phys. Chem. 113 (2000) 1698.